scientific reports

Check for updates

OPEN

Human norovirus persists longer than *Escherichia coli* in sandy soil, independent of plant decaying materials

Nuradeen Garba Yusuf[1], Courtney F. Aminirad[2], Kalmia E. Kniel[3], Sarah Strauss[4], Michelle D. Danyluk[5], Keith R. Schneider[1] & Naim Montazeri[1,6]✉

Human norovirus (HuNoV) is the leading cause of foodborne illnesses in the U.S. Fresh produce, often consumed raw, can serve as a vehicle for HuNoV transmission; however, limited data exist on its persistence in agricultural environments. This study evaluated the persistence of HuNoV GII, its cultivable surrogate Tulane virus, and *Escherichia coli* TVS 353 in sandy Florida agricultural soil. Soil samples with or without additional cilantro leaves (to simulate decaying plant debris) were incubated at 12 °C and tested for microbial concentrations at regular intervals over 29 weeks, using RNase RT-qPCR (both viruses), $TCID_{50}$ (Tulane virus), and plate count (*E. coli*). Inactivation kinetics were fitted to log-linear and non-linear models to estimate the weeks required for the first 1-log_{10} reduction (T_1D). Decaying cilantro leaves did not substantially impact microbial inactivation ($p > 0.05$). *E. coli* declined most rapidly ($T_1D = 2.2$), followed by infectious Tulane virus ($T_1D = 5.63$), Tulane virus genome copies ($T_1D = 11.8$), and HuNoV GII genome copies ($T_1D = 28$). A strong correlation of Tulane virus infectivity with HuNoV GII RNase RT-qPCR ($r = 0.82$) supported its suitability as a surrogate. Under the tested conditions, HuNoV's prolonged persistence should be accounted for in risk assessments for preharvest fresh produce production.

Keywords Agricultural soil, Enteric pathogens, Food safety, Norovirus, Public health

Human norovirus (HuNoV) is the leading cause of enteric illness outbreaks globally[1], accounting for the majority of foodborne illnesses in the U.S[2]. HuNoV is a non-enveloped, single-stranded positive-sense RNA virus from the *Caliciviridae*family[3]. Among the genetically diverse HuNoV strains, GII.4 has been consistently the most prevalent genotype associated with foodborne outbreaks in the U.S[4,5]. As an enteric pathogen, HuNoV transmits through the fecal-oral route, directly through person-to-person contact, and indirectly through consuming contaminated food or water. Its high infectivity, transmissibility, and environmental persistence make HuNoV a significant concern throughout the food supply chain[6,7].

Fruits and leafy greens are high-risk foods linked to several HuNoV outbreaks[8,9]. These foods typically do not undergo a kill step prior to consumption; therefore, preharvest practices are crucial to preventing crop contamination during production. The use of organic matter, such as animal manure and sewage treatment residuals (i.e., municipal biosolids), to enhance the nutritional quality of soil for agricultural purposes can promote the growth and survival of pathogens, posing a significant risk of pathogenic contamination for produce[10–12]. Despite the public health burden of HuNoV as a leading foodborne pathogen, the risks associated with viral persistence in agricultural soil and subsequent transfer to produce remain understudied.

[1]Food Science and Human Nutrition Department, University of Florida - Institute of Food and Agricultural Sciences, Gainesville, FL, USA. [2]Department of Microbiology and Cell Science, University of Florida - Institute of Food and Agricultural Sciences, Gainesville, FL, USA. [3]Department of Animal and Food Sciences, College of Agriculture and Natural Resources, University of Delaware, Newark, DE, USA. [4]Department of Soil, Water, and Ecosystem Sciences, Southwest Florida Research and Education Center, University of Florida - Institute of Food and Agricultural Sciences, Immokalee, FL, USA. [5]Food Science and Human Nutrition Department, Citrus Research and Education Center, University of Florida - Institute of Food and Agricultural Sciences, Lake Alfred, FL, USA. [6]Global Food Systems Institute - University of Florida - Institute of Food and Agricultural Sciences, Gainesville, FL, USA. ✉email: nmontazeri@ufl.edu

Previous studies have shown that norovirus can persist in soil for weeks to months, depending on extrinsic factors such as soil texture, organic matter, desiccation, and temperature[13–15]. Agricultural soil can serve as a vehicle for crop contamination with enteric pathogens when crops are grown directly in soil, during irrigation, rainfall events, or produce harvesting[12,16,17]. Therefore, assessing the prolonged persistence of HuNoV in agricultural soil is essential for informing produce safety guidelines and reducing the risk of foodborne transmission.

Enteric viruses, such as hepatitis A virus and HuNoV, have been isolated from naturally contaminated cilantro leaves[18], indicating potential risks for pathogen transmission to humans and the potential for cross-contamination of other crops in the field. Whether decaying plant materials in soil contribute to HuNoV persistence remains unknown. This study evaluated the persistence of HuNoV in plant-decaying materials within agricultural soil. Because no culture-based method exists for absolute quantification of HuNoV, Tulane virus, a non-human calicivirus with genetic and structural similarities to HuNoV, was used as a cultivable surrogate alongside clinical HuNoV GII to assess infectivity[19]. Tulane virus is widely recognized as a suitable cultivable surrogate for HuNoV research for inactivation studies[19–21]. Viral quantifications were based on a molecular method (RT-qPCR) for both virus groups and a culture-based assay (50% tissue culture infective dose, $TCID_{50}$) to estimate infectious Tulane virus particles[22]. The suitability of Tulane virus as a surrogate for HuNoV was evaluated by comparing inactivation kinetic parameters and the association between changes in their population densities over time.

Escherichia coli TVS 353 was included as a representative of enteric fecal bacteria, providing a practical reference for comparing bacterial and viral stability under the same conditions. Originally isolated from surface irrigation water, *E. coli* TVS 353 has been extensively used in studies on persistence and mitigation in agricultural water and soil[21,23–25]. Prior work comparing generic *E. coli* strains (TVS 353, 354, and 355) with pathogenic strains (O157 and non-O157) has shown that the generic strains exhibit greater persistence in soil environments, supporting their suitability as surrogates in field-based studies[26]. Overall, this study provides insights into the microbial hazard in produce-growing environments and supports risk-based strategies for improving prevention and mitigation of enteric pathogens in agricultural settings.

Results

Weather conditions during soil collection and baseline soil characteristics are summarized in Table 1. No target microorganisms were detected in uninoculated samples. Headspace humidity within the sealed sample bags was not measured, as soil moisture is the primary factor influencing microbial stability and was measured in the study. Initial moisture content was slightly lower in soil-only samples (4.50 ± 0.52%) than in those with decaying plant materials (5.57 ± 0.32%), though the difference was not statistically significant ($p = 0.083$). Over 29 weeks, moisture content decreased by 0.66% in soil-only samples ($p = 0.358$) and 1.6% in soil with plant materials ($p = 0.012$), with no significant difference between matrices at week 29 ($p = 0.534$). Because the entire contents of each sample bag were analyzed, these minor moisture fluctuations were not expected to influence microbial counts per gram of soil.

Microbial recovery rates are shown in Table 2. Reported microbial concentrations do not account for potential losses during the recovery process. All microbial inactivation kinetic models converged, with goodness-of-fit provided in **Supplementary Table S1**. Using the best-fit models, the marginal means of the parameters were calculated and presented in Table 3. These models enabled comparisons across microbial groups and matrices,

Source	Parameter, measuring unit	Value
Soil	pH	6.95 ± 0.15
	Potassium (K), ppm	19.32 ± 0.10
	Ammonium (NH_4N), ppm	0.32 ± 0.00
	Nitrate nitrogen (NO_3N), ppm	1.51 ± 0.04
	Total Kjeldahl nitrogen (TKN), ppm	230.65 ± 7.53
	Total Phosphorus (P), ppm	325.03 ± 25.62
	Moisture content, %	4.50 ± 0.52
	Organic matter, %	1.37 ± 0.07
	Temperature, −10 cm depth (at the collection day)*, °C	18.60 ± 2.17
	Temperature, −10 cm depth (7-day average)*, °C	19.63 ± 1.82
Weather	Relative humidity, (7-day average)*, %	77.30 ± 17.35
	Solar radiation (7-day average)*,Watts/meter^2	167.98 ± 249.86
	Temperature (at the collection day)*, °C	16.00 ± 3.94
	Temperature (7-day average)*, °C	18.34 ± 2.12

Table 1. Weather conditions during soil sample collection and baseline soil characteristics. *Data were collected from the publicly accessible database UF/IFAS Florida Automated Weather Network (FAWN) from the Live Oak, FL station, adjacent to the sample collection site, URL: https://fawn.ifas.ufl.edu. All measurements are presented as mean ± standard deviation ($n = 2$), except for 7-day averages, which were calculated from hourly records collected daily.

Microbe	Assay	Matrix	Recovery rate (%)
E. coli TVS 353	Plate count	Soil	41.65 ± 10.60
		Soil plus plant	38.63 ± 10.40
Tulane virus	$TCID_{50}$	Soil	38.27 ± 9.57
		Soil plus plant	26.07 ± 6.52
HuNoV GII	RNase RT-qPCR	Soil	47.23 ± 15.05
		Soil plus plant	46.55 ± 12.08
Tulane virus		Soil	38.61 ± 10.66
		Soil plus plant	39.28 ± 12.59

Table 2. Percentage of microbial recovery rates across each assay and matrix (mean ± standard error, $n = 3$).

Assay	Microbe	Matrix	Best fitting model	Parameters[1]	Matrix-specific estimates	Joint estimates
Plate count	*E. coli* TVS 353	Soil	*Weibull*	T_1D	2.13 [1.01, 3.25]	2.15 [1.32, 2.98]
				β	0.66 [0.53, 0.78]	0.65 [0.56, 0.74]
		Soil plus plant		T_1D	2.18 [0.96, 3.40]	
				β	0.64 [0.51, 0.77]	
$TCID_{50}$	Tulane virus	Soil	*Weibull*	T_1D	5.52 [4.42, 6.84]	5.63 [4.84, 6.41]
				β	0.81 [0.72, 0.90]	0.82 [0.76, 0.88]
		Soil plus plant		T_1D	5.73 [4.62, 6.84]	
				β	0.83 [0.74, 0.92]	
RNase RT-qPCR	HuNoV GII	Soil	*Log-linear*	T_1D	26.4 [22.5, > 30.0]	28.1 [24.9, > 30]
		Soil plus plant		T_1D	29.7 [24.8, > 30.0]	
	Tulane virus	Soil		T_1D	11.3 [10.6, 12.0]	11.8 [11.3, 12.4]
		Soil plus plant		T_1D	12.4 [11.6, 13.3]	

Table 3. Best fitting models of microbial inactivation kinetics over time, with parameter estimates and the corresponding 95% confidence intervals [lower, upper]. [1] T_1D: the time in weeks needed to achieve the first 1-$\log_{10}$ reduction in the microbial population; and β, shape parameter. Extrapolations beyond 30 weeks were avoided to minimize uncertainty in model-based estimations. These values are provided in the full model output under the supplementary materials (https://doi.org/10.5281/zenodo.16230597).

where applicable. Because the inactivation kinetics were comparable between the two matrices for all microbial targets, joint parameter estimates were also generated using the combined data.

The inactivation kinetics of *E. coli* TVS 353 were best described by the Weibull model (Table 3; Fig. 1A). None of the bacterial counts reached below the detection limit of 1.38 $\log_{10}$ CFU/g over the 29-week study period. Estimated T_1D values were similar in the soil plus plant materials (2.18 weeks [95% CI: 0.96, 3.40]) and soil-only samples (2.13 weeks [95% CI: 1.01, 3.25], $F_{1, 113} = 0.004$, $p = 0.951$), corresponded to a combined T_1D value of 2.15 weeks [95% CI: 1.32, 2.98]. The shape parameter β, reflecting curvature of the Weibull model, did not differ significantly between matrices ($F_{1, 113} = 0.035$, $p = 0.852$) and was estimated at 0.65 [95% CI: 0.56, 0.74] for combined data. When models were refitted to estimate the time for the first two- and three-decimal reductions (T_2D and T_3D), the corresponding values across both matrices were 6.28 weeks [95% CI: 4.74, 7.81] and 11.70 weeks [95% CI: 9.79, 13.70], respectively.

Similar to *E. coli* TVS 353, Tulane virus infectivity, measured by $TCID_{50}$ assay, was best fitted with the Weibull model (Table 3; Fig. 1B). No substantial heteroscedasticity was detected, so variance functions were not necessary. The estimated T_1D value was 5.73 weeks [95% CI: 4.62, 6.84] in soil plus plant materials and 5.52 weeks [95% CI: 4.84, 6.84] in the soil-only samples, with no significant difference between matrices ($F_{1, 113} = 0.07$, $p = 0.790$), resulting in the combined T_1D of 5.63 weeks [95% CI: 4.84, 6.41]. Furthermore, the respective T_2D and T_3D values were 13.1 weeks [95% CI: 12.1, 14.1] and 21.5 weeks [95% CI: 20.5, 22.5], indicating a slower viral decline than bacterial inactivation. The shape parameter β did not differ between matrices ($F_{1, 113} = 0.08$, $p = 0.781$), with a combined estimate of 0.82 [95% CI: 0.75, 0.88], indicating a moderately convex inactivation (tailing) curve. Although the concentrations stayed above the detection limit of 0.50 $\log_{10}$ $TCID_{50}$/g, a tail-like persistence phase emerged near the end of the 29-week period.

Tulane virus and HuNoV GII were quantified using RNase RT-qPCR. Both remained detectable throughout the trials, and their inactivation kinetics were best described by the log-linear model by incorporating an exponential variance structure to improve the fit and correct the residual heteroscedasticity (Table 3; Fig. 2). Consistent with previous conditions, no significant difference in T_1D values was observed across matrices ($F_{1, 230} = 1.90$, $p = 0.173$), corresponded to the estimated T_1D values of 11.8 weeks [95% CI: 11.3, 12.4] for Tulane virus and 28.1 weeks [95% CI: 24.9, > 30] for HuNoV GII. The substantially higher T_1D value for HuNoV GII reflects its greater persistence ($F_{1, 230} = 98.50$, $p < 0.0001$). The estimated T_2D value was 23.7 weeks[95% CI: 22.58, 24.83]

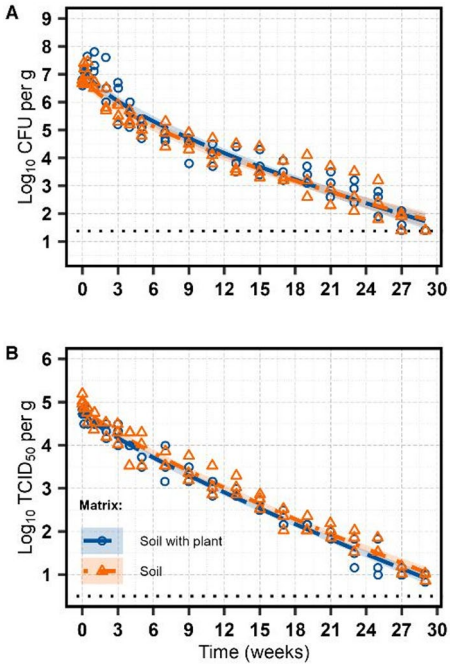

Fig. 1. Inactivation of *E. coli* TVS 353 (**A**) and Tulane virus (**B**) in sandy soil plus plant and sandy soil-only sample over 29 weeks at 12 °C, quantified with total plate count and $TCID_{50}$, respectively ($n = 3$). The best fit is illustrated by the dot-dashed and dashed lines for the soil-only sample and soil plus plant, respectively. Shaded areas represent 95% confidence intervals. The horizontal dotted line marks the detection limits of 1.38 $\log_{10}$ CFU/g for *E. coli* TVS 353 and 0.50 $\log_{10}$ $TCID_{50}$/g for Tulane virus.

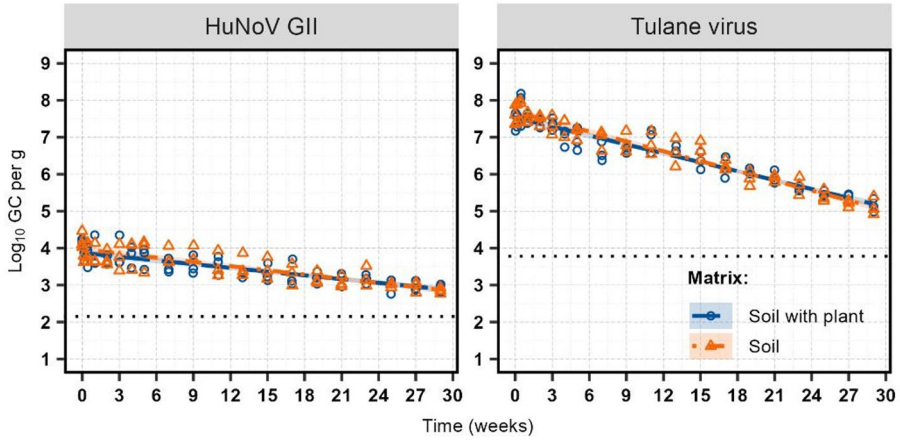

Fig. 2. Inactivation of HuNoV GII and Tulane virus in sandy soil plus plant and sandy soil-only control samples over 29 weeks at 12 °C, quantified using RNase RT-qPCR ($n = 3$). Fitted values from the joint reparametrized log-linear models are represented as dashed lines for the soil plus plant sample and dot-dashed lines for the soil-only control sample. Shaded areas represent 95% confidence intervals. Dotted lines indicate the detection limits of 2.15 $\log_{10}$ GC/g for HuNoV GII and 3.78 $\log_{10}$ GC/g for Tulane virus.

for Tulane virus, while HuNoV GII exceeded 30 weeks. For both viruses, achieving a T_3D required more than 30 weeks.

We observed a nearly linear positive correlation between T_1D and the β parameters in Weibull models for *E. coli* TVS 353 and Tulane virus infectivity. Parametric Monte Carlo simulations using the joint variance–covariance matrix (joint draws) confirmed that the observed correlation mainly affected the width of T_1D confidence intervals, not central estimates. Independent-parameter simulations (assuming zero covariance) further inflated uncertainty, and in only one case, RNase RT-qPCR data for Tulane virus in the soil-only matrix, it produced negative bounds, though T_1D estimates remained stable (**Supplementary Table S2**).

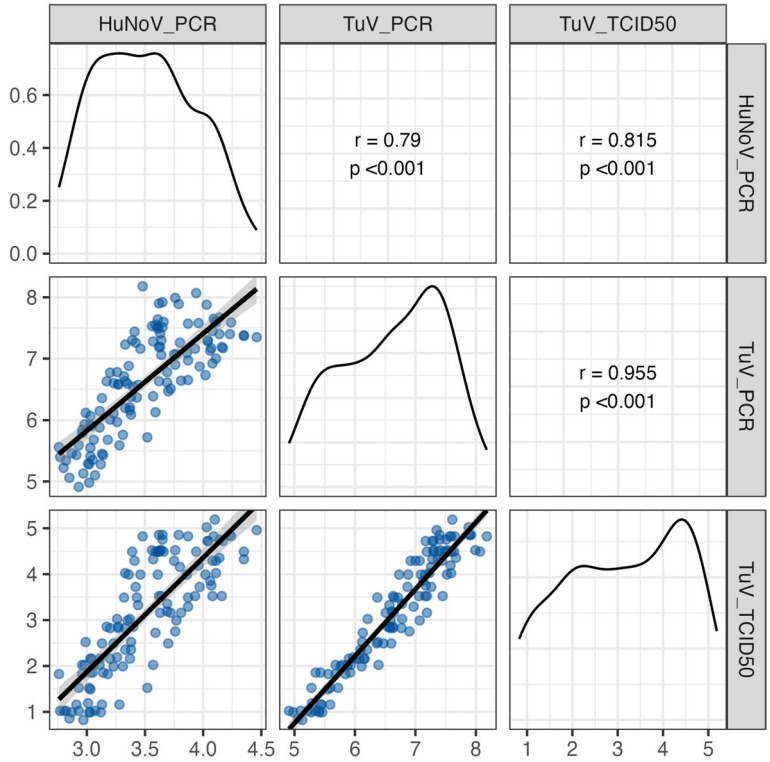

Fig. 3. Pairwise correlation matrix of viral concentrations across experimental conditions (virus groups and assays). The lower triangle panels show scatterplots with fitted linear regression lines and shaded 95% confidence intervals. The upper triangle panels display Pearson's product-moment correlation coefficients (r) with corresponding p-values. Diagonal panels present kernel density plots of viral concentrations for each condition.

The $\log_{10}$ GC: $TCID_{50}$ ratio was used to compare Tulane virus quantification by RNase RT-qPCR and infectivity assay. At inoculation, the ratio was 2.62 ± 0.10 in both matrices ($p = 0.535$), then increased over time in both matrices, reaching 4.18 ± 0.09 by the end of the study ($p = 0.805$). No main effect of matrix was observed ($F_{1, 49.2} = 1.30$, $p = 0.263$), but time had a significant effect ($F_{19, 4.4} = 37.30$, $p = 0.001$), indicating a progressive loss of infectivity relative to detectable virus particles with intact capsid. No significant matrix-by-time interaction was observed ($F_{19, 4.4} = 1.10$, $p = 0.518$).

To evaluate Tulane virus suitability as a surrogate for HuNoV GII, a Pearson correlation matrix was generated across virus types and quantification methods (Fig. 3). The strongest correlation was observed between the Tulane virus $TCID_{50}$ assay and its RNase RT-qPCR measurements ($r = 0.96$, $p < 0.001$), indicating high consistency across detection platforms. A strong positive correlation was also found between the RNase RT-qPCR data for HuNoV GII and the infectivity assay for Tulane virus ($r = 0.82$, $p < 0.001$), suggesting similar behavior between the two viruses under the tested conditions. Tulane virus and HuNoV GII RNase RT-qPCR data showed a moderate correlation ($r = 0.79$, $p < 0.001$). Collectively, these findings support the use of Tulane virus infectivity data to track relative changes and trends in HuNoV.

Discussion

The prolonged persistence of enteric pathogens in fecally contaminated soil increases the likelihood of crop contamination during preharvest stages[8,10–12]. To address the knowledge gap on persistence of enteric viruses in agricultural soil, we conducted a persistence study using HuNoV GII, its cultivable surrogate Tulane virus, and *E. coli* TVS 353, a non-pathogenic enteric bacterial model, in agricultural sandy soil with or without the addition of decaying plant materials. Microbial decay kinetics were modeled using linear and non-linear models. Deviations from log-linear inactivation are common in environmental matrices due to aggregation, adsorption, organic matter protection, or the presence of resistant subpopulations[27–29]. Non-linear models are increasingly favored as they better capture transition dynamics and provide more robust insights into pathogen survival than log-linear models, which often underestimate persistence at low concentrations[26,30]. We observed high correlations between Weibull parameter estimates, commonly reported due to mathematical dependencies between shape and scale parameters[31–33]. Although this dependency inflates parameter variances and covariances, the model can still produce nearly symmetric confidence intervals[31,32]. Incorporating the full variance–covariance matrix when computing estimated marginal means, as performed here, improves confidence interval accuracy, particularly under strong collinearity[32,34].

The persistence of enteric pathogens in soil is shaped by both extrinsic and intrinsic factors, including soil texture, temperature, pH, salinity, organic content, microbial community composition, and the specific bacterial strain[27,35–37]. This study was conducted in highly sandy soil at a constant temperature of 12 °C in the dark. Storage below 8 °C or above 15 °C often results in two-stage (biphasic) kinetics, whereas intermediate temperatures tend to suppress this behavior[38]. A meta-regression analysis of studies on *E. coli* survival in soil at 4 °C to 38 °C showed that higher temperatures yielded a slower inactivation for nonpathogenic strains (0.90 $\log_{10}$ CFU per week) than for pathogenic strains (0.92 $\log_{10}$ CFU per week), indicating a moderate temperature effect[39].

In this study, *E. coli* TVS 353 remained detectable throughout the 29-week period, and decaying plant material (cilantro leaves) had no significant effect on microbial persistence. Its inactivation in both matrices combined was best described by the Weibull model, with a combined T_1D of approximately 2.2 weeks. This result agrees with reported T_1D values of 2 weeks for *E. coli* on leafy greens[40] and 2–8.6 weeks for *E. coli* O157:H7 in fresh produce growing soils[36]. A related laboratory-based study on*E. coli* O157:H7 strains in natural sandy soil from the same field reported a T_1D of less than one week at 30 °C, with counts declining from approximately 7 $\log_{10}$ CFU/g to below the 0-$\log_{10}$ CFU/g limit of detection in 8 weeks[25]. In that work, autoclaving the soil reduced indigenous microbes and prolonged *E. coli* survival, with extinction (negative enrichment) occurring at week 24 versus 12 weeks in natural soil.

Although the bacterial population remained detectable throughout the study, the reduction observed in samples may partly explained by the ability of bacteria to enter a viable but non-culturable (VBNC) state. This adaptive mechanism, also documented for *E. coli* O157:H7, enables subpopulations to persist in a viable yet undetected form by standard culture-based methods[41]. Because no complementary viability assays were performed for *E. coli* TVS 353, the fraction of undetectable cells in a VBNC remains unknown. Consequently, the observed decline in culturable counts may not fully reflect the survival of viable cells, and the term persistence for *E. coli* in this context should be more precisely interpreted as culturability.

A 4-week study reported that *E. coli* TVS 353 in both amended and unamended soils from Beltsville, MD, U.S. (used during organic lettuce production in box planters at 20 °C) followed a log-linear model (T_1D = 0.9 weeks), while *E. coli* O157:H7 strains were best described with Weibull[27]. That study also concluded biologically amended soil may support, but does not necessarily enhance, *E. coli* survival. Both strains showed T_3D values within 3 weeks, whereas our data estimated 11.7 weeks to achieve a similar reduction. This finding is consistent with prior reports of greater persistence of TVS strains compared with pathogenic strains[26].

Quantification of viral particles using culture-based and molecular methods, where applicable, provided insights into infectivity and the viral integrity in soil[19,42]. As shown with *E. coli* TVS 353, decaying cilantro leaves had no effect on HuNoV and Tulane virus persistence over 29 weeks. Faster reductions of murine norovirus (another HuNoV surrogate) and Tulane virus have been reported on spinach leaves grown in pots at 18 °C and 65% relative humidity (T_1D of 0.7–0.8 weeks)[43], and on the adaxial leaf surfaces of 4-week-old pre-harvest basil plants grown at 24 °C and 43% relative humidity (T_1D of 0.4 weeks)[44]. These rapid declines were attributed to potential effects of plant-derived antiviral compounds, irreversible attachment of virus particles to plant-derived antiviral compounds, irreversible attachment, or internalization that prevented virus recovery for accurate enumeration[43,44].

In contrast to *E. coli* TVS 353, both HuNoV and Tulane virus showed slower decay in soil samples. Tulane virus infectivity, measured by $TCID_{50}$, declined with a T_1D of 5.63 weeks, with T_2D and T_3D reached at 13.1 and 21.5 weeks, respectively. By comparison, murine norovirus in sandy and loamy soils showed faster inactivation by plaque assay, with T_1D of approximately 2 weeks, followed by T_2D of 3 weeks, and then reached the 1 $\log_{10}$ PFU/ml limit of detection in 5.5 weeks[15]. Another research on Tulane virus survival in gravelly loam soil demonstrated a 2–2.5 $\log_{10}$ reduction over 4 weeks, with a detectable virus titer by the end of the study period[45].

This study used a $TCID_{50}$ assay to assess changes in Tulane virus infectivity over time. Although widely applied, this method is generally considered less precise, offering lower sensitivity and no absolute quantification[22]. Nevertheless, Tulane virus remained detectable throughout the 29-week study, with levels above the 0.5 $\log_{10}$ $TCID_{50}$/g detection limit. Using a $\log_{10}$ $TCID_{50}$:PFU conversion ratio of − 0.65 [95%CI: −1.15, − 0.16][22], this limit corresponds to approximately 1.15 $\log_{10}$ PFU/g [95%CI: 0.66, 1.65]. Based on this conversion, the final titer of 0.96 $\log_{10}$ $TCID_{50}$/g observed in both matrices equates to 1.61 $\log_{10}$ PFU/g [95%CI: 1.12, 2.11], approximating residual infectious particles near the tailing phase. Notably, the original ratio was derived from 96-well plate assays, while this study used 48-well plates, a methodological variation that may slightly affect conversion due to assay sensitivity.

RNase RT-qPCR quantification of Tulane virus yielded titers approximately 3.5 $\log_{10}$ units higher than $TCID_{50}$, reflecting detection of both infectious and intact but non-infectious particles[22,46]. Persistence data obtained from RNase RT-qPCR were best fit by the log-linear decay model, which estimated longer T_1D values of 28.1 weeks for HuNoV GII and 11.8 weeks for Tulane virus across both matrices. Because RNase depends on capsid degradation to expose viral RNA to enzymatic digestion, it cannot detect earlier mechanistic losses of infectivity, such as impaired receptor-binding[46], likely explaining the slower observed inactivation kinetics. Virus aggregation or particle binding may also underestimate infectivity by altering apparent kinetics[29], yet these particles can still be lysed during RNA extraction, allowing detection by RNase RT-qPCR. This independence from the particle state may partly explain the log-linear decay observed in molecular data.

Based on RNase RT-qPCR data, HuNoV GII required approximately 16.3 weeks longer than Tulane virus to reach the first $\log_{10}$ reduction, consistent with reviews reporting greater environmental resistance of HuNoV compared to its surrogates under similar stress[42]. Beyond intrinsic stability, HuNoV aggregation and particulate association matter in stool may contribute to its prolonged persistence in environmental matrices[29]. In contrast, monodispersed Tulane virus preparations used here[22] may have enabled faster inactivation by enhancing virus exposure to extrinsic factors[29], establishing a baseline for decay under the most vulnerable physical state. Other

forms, such as vesicle-associated or cloaked clusters, may enhance stability; however, their protective role remains to be elucidated[47].

This study observed a strong correlation between Tulane virus infectivity and RNase RT-qPCR data across both matrices (r = 0.96), indicating that RNase RT-qPCR reliably captured relative changes in Tulane virus persistence. A higher correlation (r = 0.99) was previously reported forserially diluted Tulane virus in buffer when comparing RNase RT-qPCR to plaque assay results[22], likely due to the higher sensitivity of plaque assays and absence of virus-associated matrix effects. By contrast, the correlation between RNase RT-qPCR data for HuNoV GII and Tulane virus was moderate (r = 0.79), suggesting assay performance may vary by virus type. The correlation between HuNoV RNase RT-qPCR data and Tulane virus infectivity was slightly stronger (r = 0.82), reflecting a consistent association between the two assays in capturing overall inactivation trends.

Infectivity and RNase RT-qPCR data for Tulane virus suggest that prolonged persistence in soil, with or without plant materials, leads to loss of infectivity without major capsid degradation. These findings support the use of RNase pretreatment to improve the interpretation of RT-qPCR data for assessing virus viability. However, each method captures distinct aspects of virus integrity and must be interpreted within the context of its limitations[48]. As demonstrated here, strong correlations among quantification methods do not imply that the underlying inactivation kinetics, or the apparent decay rates, are directly comparable. To enhance biological relevance, future work should integrate viability assays and culture-based methods to strengthen the interpretation of persistence data and inform evidence-based guidelines for preventing viral contamination in fresh produce.

Conclusions

This study addresses key gaps in the environmental stability of enteric pathogens relevant to preharvest produce safety. Using sandy soil from a Florida research farm, we evaluated the persistence of HuNoV GII, its surrogate Tulane virus, and *E. coli* TVS 353, while testing the influence of decaying plant material on inactivation kinetics. Molecular (RNase RT-qPCR) and culture-based (plate count and $TCID_{50}$) quantification methods revealed distinct microbial- and assay-specific decay kinetics. Culture-based assays showed Tulane virus persisted much longer than *E. coli* TVS 353, highlighting the widely recognized environmental stability of enteric viruses. Under the tested conditions, Tulane virus served as a reliable surrogate for HuNoV GII, supported by a strong correlation between Tulane virus infectivity and HuNoV RNase RT-qPCR data. However, RNase RT-qPCR data suggested greater capsid stability for HuNoV GII relative to Tulane virus. Whether this structural integrity translates into prolonged HuNoV infectivity remains uncertain and warrants direct culture-based infectivity assays for HuNoV. Although conducted at a single temperature (12 °C) under controlled conditions (without sunlight or other environmental factors), this study provides valuable insights by using actual agricultural soil as the test matrix. Decaying cilantro leaves, at the tested levels, had no measurable effect on microbial decay. All microorganisms remained detectable throughout the 29-week period, signifying the potential for agricultural soils to serve as long-term reservoirs for enteric pathogens, particularly enteric viruses.

Materials and methods

Sample collection and soil quality analysis

Agricultural soil samples were collected in March 2024 from the University of Florida North Florida Research & Education Center – Suwannee Valley (Live Oak, FL, USA). The site was historically used for cultivating a variety of vegetables, including watermelon, tomatoes, and peppers. Weather and soil condition data were collected from the UF/IFAS Florida Automated Weather Network (FAWN) database, publicly accessible at https://fawn.ifas.ufl.edu.

All instruments were sanitized with 70% alcohol prior to use. Approximately 20 kg of soil was collected at a 15 cm depth and stored at 4 °C for up to one week before quality parameters were measured. To represent plant decaying materials, soil samples were tested for microbial persistence with and without the presence of cilantro (*Coriandrum sativum*) leaves. Fresh cilantro leaves with branches were purchased from local grocery stores in Gainesville, FL, and used without further washing.

Soil properties were measured on the original soil samples, except moisture content, which was determined in soil-only samples and those mixed with plant materials. Particle size distribution classified the soil as highly sandy[49], with 94.9% sand, 3.1% silt, and 2.0% clay. Soil properties, except moisture content, were analyzed by the University of Florida IFAS Analytical Services Laboratory (Gainesville, FL). Soil pH was determined using the EPA Method 150.1 with an Orion Versa Star™ meter (Thermo Scientific, USA)[50]. Potassium was measured using EPA Method 200.7[51] by inductively coupled plasma optical emission spectrometry (ICP-OES). Ammonium-nitrogen (NH_4-N) was measured using a modified U.S. EPA Method 350.1[52]. Nitrate-nitrogen (NO_3-N) was determined using U.S. EPA Method 353.2[53]. Total Kjeldahl nitrogen (TKN) was determined using U.S. EPA Method 351.2[54] using an OI Analytical Flow Solution FS3700 Automated Chemistry Analyzer (Xylem Inc., Washington, DC). Total phosphorus was measured using U.S. EPA Method 365.1[55], also with the OI Analytical Flow Solution FS3700 system. Soil moisture content was determined using a gravimetric method[56], and organic matter content was assessed using the loss on ignition method described elsewhere[57].

Preparation of microbial stocks

Rifampicin-resistant *E. coli* TVS 353, originally isolated from surface irrigation water, was obtained from K. Schneider at the University of Florida (Gainesville, FL). Stock cultures were grown in brain heart infusion (BHI) broth (BD BBL™, Sparks, MD, USA) with 80 µg/mL rifampicin (TCI America™, St. Portland, OR, USA), and stored with 30% glycerol at −80°C[25]. Working stocks were prepared from colonies grown on BHI-rifampicin agar, stored at 4 °C, and refreshed biweekly. For each inoculation, a single colony was transferred into BHI-

rifampicin broth and incubated at 37 °C for 24 ± 2 h with shaking at 150 rpm. A 1 mL of culture was centrifuged at 8,000 ×g for 3 min, resuspended in 1 mL of phosphate-buffered dilution water (PBDW, pH 7.2; Alpha Biosciences, Baltimore, MD, USA), reaching a final concentration of approximately 9 $\log_{10}$ CFU/mL, and used for inoculation.

Tulane virus was provided by L.A. Jaykus at North Carolina State University (Raleigh, NC) and propagated in rhesus monkey kidney cells (LLC-MK2, ATCC CCL-7™) at a multiplicity of infection of 0.1. Infected cells were incubated at 37 °C with 5% CO_2 in Opti-MEM™ medium (Gibco Life Technologies, Grand Island, NY, USA) supplemented with 2% fetal bovine serum (FBS, Gibco™, Thermo Fisher Scientific, USA), 1× antibiotic-antimycotic solution, 0.22% sodium bicarbonate, and 1× GlutaMAX™ (all from Gibco Life Technologies). Once cytopathic effects were observed, lysates were harvested, purified through iodixanol-based discontinuous gradient ultracentrifugation (OptiPrep™, Cosmo Bio USA, Carlsbad, CA), and resuspended in 10 mM Tris-1 mM EDTA buffer (pH 7.5), as described[22]. Purified stocks were stored at − 80 °C. Viral infectivity was later determined using the $TCID_{50}$ assay as described below. The final suspension reached a titer of approximately 9.2 $\log_{10}$ $TCID_{50}$/mL and was previously confirmed to contain primarily monodispersed particles[22].

A diluted HuNoV GII-positive human stool specimen, from a symptomatic individual, was prepared as previously described[58], served as the source of the virus stock. Presence of HuNoV GII at ~ 8.0 $\log_{10}$ Genome Copies (GC)/g was confirmed using the RNase RT-qPCR method described below. Briefly, the stool was suspended at a 1:5 ratio in PBDW (pH 7.2; Alpha Biosciences), vortexed at high speed for one minute, and centrifuged twice at 3,100 × g for 2 min. The clarified supernatant was aliquoted, stored at − 80 °C, and used as needed.

Sample inoculation and storage

Experiments were performed in triplicate, with each microbial assay measured in duplicate. Ten grams of soil were placed in a 12.5 by 7.5 cm Whirl-Pak™ bag (Fisher Scientific, Waltham, MA, USA), which was equipped with a built-in leak-proof closure tab. A microbial cocktail was first prepared by combining 100 µL of Tulane virus working stock, 5µL of clarified HuNoV GII stool suspension, and 50 µL of *E. coli* TVS 353. Ten to thirteen cilantro leaves (approximately 0.75 g) were then each spot-inoculated with a 10-µL aliquot of the cocktail. Inoculating with a cocktail minimized potential matrix effects from the stool-derived HuNoV GII preparation and allowed a more consistent comparison of environmental stability across the three microorganisms.

Leaves were left under a biosafety cabinet for 60 min to allow the inoculum to dry and facilitate microbial attachment[59], then were transferred to soil and hand-massaged for 30 s to settle the plant material at the bottom to decay. Inoculated soil with or without cilantro leaves contained initial concentrations of 5 $\log_{10}$ $TCID_{50}$/g and 7.9 $\log_{10}$ GC/g for Tulane virus, 4 $\log_{10}$ GC/g for HuNoV, and 7 $\log_{10}$ CFU/g for *E. coli* TVS 353, as represented by week zero of the study period. For soil-only control, soil was inoculated with the same microbial cocktail, left for 60 min to permit adsorption, then mixed by hand. Microbial analyses were performed at days 0, 1, and 3, weekly from weeks 1 to 5, then biweekly from weeks 7 to 29. These time points allowed accurate kinetic modeling of microbial inactivation over time.

All bags were folded, sealed, and incubated under dark conditions at 12 °C in a refrigerated incubator for 29 weeks. This temperature reflects the lower bound of the U.S. FDA/EPA recommended water temperature range (12 °C and 32 °C) for testing sanitizer efficacy in preharvest agricultural water[60] and matches conditions from a previous HuNoV and *E. coli* TVS 353 persistence study in preharvest water[61]. This temperature also approximates the average soil temperature of 18.2 ± 5.0 °C observed in Florida's cool season from October to March (**Supplementary Fig. S1**)[62], ensuring relevance to regulatory guidelines and supporting the integrated assessment of microbial risks in agricultural systems.

Microbial recovery

Microbial recovery was performed based on the FDA Bacteriological Analytical Manual (BAM), which details the recovery of HuNoV and hepatitis A virus from green onions and leafy greens, after some modifications[63]. Major modifications included the change in elution buffer and the use of size exclusion filters instead of ultracentrifugation for the virus recovery. Briefly, the content of each sampling bag was transferred into a sterile 15 by 23 cm Whirl-Pak™ filter bag (Fisher Scientific), containing 30 mL of TGBE (pH 9.0) elution buffer, composed of 0.1 M Tris-base (Fisher Chemical, Ottawa, ON, Canada), 0.05 M glycine (Fisher Scientific, Geel, Belgium), and 10% (*w/v*) beef extract (Gibco Life Technologies, Detroit, MI, USA). Target organisms were eluted by mixing the content in a Stomacher® 80 Biomaster (Seward Inc., NY, USA) for 30 s at the normal setting. To minimize debris carryover, the eluate was carefully recovered from the side of the filter bag and transferred into sterile tubes. A 1-mL aliquot of the eluate was immediately taken for *E. coli* TVS 353 enumerations by spreading 0.1 mL of undiluted and serially diluted samples on BHI-rifampicin agar, as explained earlier.

The remainder of the microbial elute was further processed for virus testing. First, samples were centrifuged at 12,000 × g for 20 min at 18 °C using an Allegra® 64R benchtop centrifuge (Beckman Coulter Life Sciences, Indiana, USA). Then, the supernatants were concentrated using Amicon™ Ultra-15 Centrifugal Filter Units (MilliporeSigma™, Merck Millipore Ltd., Co Cork, Ireland) at 4,500 × g for 30 min at 18 °C before storage at − 80 °C. Prior to analysis, freshly thawed samples were sonicated in an ultrasonic bath at 150 W (40 kHz) for 4 min (Branson®, Model CPX1800H, Mexico) to reduce particle aggregation and virus-particle binding, as previously described[22,58]. This treatment did not adversely affect bacterial or viral viability. Microbial recovery rates (%) were determined at week zero by calculating the ratio of total microbes recovered to those added to samples.

Microbial quantification

Samples were analyzed either undiluted or after serial dilutions. For the *E. coli* quantification, a 100 µL aliquot of each sample was plated onto BHI-rifampicin agar (Fisher Scientific) and incubated at 37 °C for 24 h. After

incubation, visible colonies were enumerated. The detection limit was 1.38 $\log_{10}$ CFU/g. The infectivity of Tulane virus was assessed using the $TCID_{50}$ assay, following a previously described method with minor modifications[22]. Virus samples were serially diluted in Opti-MEM™ medium (OptiPrep™, Cosmo Bio USA, Carlsbad, CA) supplemented with 1× antibiotic-antimycotic (Gibco Life Technologies, Grand Island, NY, USA), 2.94% (*v/v*) sodium bicarbonate (Gibco), and 1× GlutaMAX™ (Gibco Life Technologies). For each dilution, including undiluted samples, 120 µL was added to four replicate wells of a 48-well Nunc™ MicroWell™ plate (Thermo Fisher Scientific), each seeded with a 90% confluent monolayer of LLC-MK2 cells. Plates were incubated at 37 °C in a humidified 5% CO_2 atmosphere for 1 h to allow virus adsorption, with gentle rocking every 15 min to ensure uniform distribution.

Following adsorption, 280 µL of Opti-MEM™ medium supplemented with 2% (*v/v*) FBS (Thermo Fisher Scientific) and an antifungal additive (Fungin™, InvivoGen, San Diego, CA, USA) was added to each well. Plates were incubated until cytopathic effects (CPE) were observed. Then, cells were fixed with 3.7% (*v/v*) formaldehyde (Thermo Fisher Scientific) and stained using 0.1% (*w/v*) crystal violet (Sigma-Aldrich, St. Louis, MO). Infectious virus titers, expressed as $\log_{10}$ $TCID_{50}$/g, were calculated using the Reed-Muench method[64], based on the proportion of wells showing CPE at each dilution. The assay's detection limit was 0.50 $\log_{10}$ $TCID_{50}$/g, corresponding to CPE observed in two of four replicate wells with undiluted samples.

To assess potential infectivity by targeting intact viral capsids, each 200-µL sample was treated with 1 U of RNase ONE™ (Promega, Madison, WI), as previously described[65]. Viral RNA was extracted using the QIAamp Viral RNA Mini Kit (Qiagen, Hilden, Germany), following the manufacturer's instructions. Extracted RNA was analyzed in duplicate using the Luna® Universal Probe One-Step RT-qPCR Kit (New England Biolabs, Ipswich, MA) on a CFX96 Touch™ Real-Time PCR System (Bio-Rad, Hercules, CA).

Each 25-µL RT-qPCR reaction contained 1× reaction mix, 1× enzyme mix, 25 U murine RNase inhibitor (New England Biolabs), 0.25 µM of each primer and probe, and 3 µL of RNA template. Separate assays were run for each virus using specific primers and probes: TVF/TVR/TVP for Tulane virus[66] and JJV2F/COG2R/RING2P for HuNoV GII[67,68]. Thermal cycling conditions followed previously validated protocols[58]. Viral genome copies (GC) were quantified by generating standard curves from serial dilutions of RNA transcripts, in line with established methods[58]. To mitigate PCR inhibition, likely caused by co-extracted humic substances from soil and residual beef extract used during virus recovery[69], all reactions were performed using a 1:10 dilution of the extracted template, and this dilution factor was incorporated into the final quantification. The detection limits were 3.78 $\log_{10}$ GC/g for Tulane virus and 2.15 $\log_{10}$ GC/g for HuNoV, based on a cycle threshold (Ct) cutoff of 40[22].

Statistical analysis and decay kinetics modeling

This study estimated microbial decay in soil plus plant (treatment) relative to soil-only (control). Estimated parameters are presented as marginal means ± standard error or with 95% confidence or quantile intervals [lower, upper], where applicable. Statistical analysis was conducted in RStudio version 4.5.0[70]. Data entry and initial preprocessing were performed using open-source R packages *tidyverse*[71] and *here*[72].

Inactivation kinetics of microorganisms were modeled jointly for each assay technique to allow statistical comparisons across microbial types and soil matrices, where applicable. Both linear and biologically relevant nonlinear models, the Weibull and $\log_{10}$-logistic, were fitted using generalized nonlinear least squares via the *nlme* package[73]. The log-linear model assumes first-order kinetics, assuming a constant microbial inactivation rate over time. Conversely, the Weibull model describes a continuous change in decay over time. The β parameter in a Weibull model distinguishes between linear ($\beta = 1$), concave ($\beta > 1$), indicating a tailing, and convex ($\beta < 1$), indicative of a shoulder[31]. The $\log_{10}$-logistic model assumes a $\log_{10}$-normal-like distribution of variability in microbial resistance to inactivation and has been used extensively in persistence and inactivation studies[21,74,75]. The reparametrized forms of the log-linear (Eq. 1) and Weibull (Eq. 2) models were based on previous studies[28,76]. The $\log_{10}$-logistic model (Eq. 3) was reparametrized according to our previous study[21].

Unlike log-linear kinetics, decimal reduction time is not constant in non-linear models. Through reparameterization, we replaced the model's decay rate with the $T_{\Delta}D$ parameter, defined as the time in weeks required to achieve the first Δ-$\log_{10}$ reduction in microbial count. A larger $T_{\Delta}D$ value, therefore, corresponds to slower decay and thus a longer persistence. The time for the first $\log_{10}$ (90%) reduction, T_1D, was used as a comparative benchmark to evaluate initial decay across different microbial targets and matrices. The models were also refitted to estimate T_2D and T_3D, providing context on longer-term microbial decline. Because $T_{\Delta}D$ alone cannot accurately estimate microbial population density at a given time, it is crucial to utilize the entire fitted model for prediction. Since the microbial inactivation kinetics may not remain consistent after 29 weeks, extrapolation beyond 30 weeks was avoided to minimize uncertainty in model-based estimations.

$$(\log - \text{linear}) : log_{10}\ (N_t) = log_{10}\,(N_0) - \ \Delta\ \left(\frac{time}{T_{\Delta}\,D}\right) \tag{1}$$

$$(\text{Weibull}) :\ log_{10}\,(N_t) = log_{10}\,(N_0) - \Delta\ \left(\frac{time}{T_{\Delta}\,D}\right)^{\beta} \tag{2}$$

$$(\log_{10} - \text{logistic}) : log_{10}\,(N_t) = log_{10}\,(N_0) - log_{10}\left(1 + e^{\left(\frac{\ln(time) - [\ln(T_{\Delta}\ D) - \ln(10^{\Delta}\ -1) \times\ \sigma^{\ 2}]}{\sigma^{\ 2}}\right)}\right) \tag{3}$$

where:

- *time*: incubation time (weeks),
- Δ: number of decimal reductions in microbial count,
- $T_{\Delta}D$: time in weeks required to achieve the first Δ $\log_{10}$ reductions in microbial count,
- β: shape parameter, and
- σ: variability in the population's sensitivity to inactivation.

A null model was implemented by specifying constant parameters across the assays, assuming no effect of the matrix variable. This intercept-only model served as a baseline for comparison against more complex models incorporating matrix-specific parameters. The second-order Akaike's Information Criterion (AICc) from the *performance* package[77] was used to assess the goodness-of-fit, with penalties applied for models with more parameters to avoid overfitting. A model with an AICc at least two units lower than that of competing models was considered the best fit[78]. Model adequacy was further assessed by comparing residual diagnostic plots between the null and full models using the *ggResidpanel* package[79], and variance functions from the *nlme* package were applied as needed to address heteroscedasticity[73]. The model with the lowest AICc and acceptable residual diagnostics was selected for statistical inference.

Statistical inference and interpretation

Model coefficients and their associated uncertainties were estimated from the best-fitting models, followed by pairwise post-hoc comparisons and contrasts using the *emmeans* package[34]. Marginal means of estimated values across incubation weeks were determined with the *marginaleffects* package[80]. Because the fitted parameters showed notable correlation, a parametric Monte Carlo simulation was performed by drawing 5,000 coefficient vectors from the model-specific multivariate normal distribution using the *MASS* package[81], preserving the full variance–covariance structure to assess its impact on level-specific T_1D estimates. For each draw, T_1D at each level (or level combination) was reconstructed from the appropriate linear combination of T_1D coefficients; simulated means and 95% QIs were compared with the marginal means previously estimated from the established models. As a sensitivity analysis, the simulation was repeated with a diagonalized covariance matrix (off-diagonals set to zero) to approximate independent coefficients.

When applicable, observed data were subjected to pairwise comparisons across time points using the *multcomp* and *multcompView* packages[82,83], with the significance level set at $\alpha = 0.05$. Pearson's correlation coefficients were calculated to assess similarities between virus groups and quantification methods. A correlation matrix was generated using the *GGally* package[84]. Additionally, the $\log_{10}$ GC: $TCID_{50}$ ratio for Tulane virus was computed to assess the proportion of RNase RT-qPCR signalattributable to infectious particles[22]. This ratio supports the interpretation of molecular results in the context of risk assessment and validation of surrogate virus performance.

Data availability

The dataset generated and analyzed during the current study, along with the R scripts and their outputs, are available in the publicly accessible Zenodo repository at https://doi.org/10.5281/zenodo.16230597.

Received: 26 August 2025; Accepted: 4 December 2025
Published online: 15 December 2025

References

1. Kirk, M. D. et al. World health organization estimates of the global and regional disease burden of 22 foodborne bacterial, protozoal, and viral diseases, 2010: a data synthesis. *PLoS Med.* **12**, e1001921 (2015).
2. Scallan Walter, E. J. et al. Foodborne illness acquired in the united States—major pathogens, 2019. *Emerg Infect. Dis.* **31**, 7–15 (2025).
3. Chhabra, P. et al. Updated classification of norovirus genogroups and genotypes. *J. Gen. Virol.* **100**, 1393 (2019).
4. Barclay, L. et al. Molecular evolution and epidemiology of norovirus GII.4 viruses in the united States. *J. Infect. Dis.* **jiaf100** https://doi.org/10.1093/infdis/jiaf100 (2025).
5. Hardstaff, J. L. et al. Foodborne and food-handler norovirus outbreaks: a systematic review. *Foodborne Pathog Dis.* **15**, 589–597 (2018).
6. De Graaf, M., Van Beek, J. & Koopmans, M. P. G. Human norovirus transmission and evolution in a changing world. *Nat. Rev. Microbiol.* **14**, 421–433 (2016).
7. Wikswo, M. E. et al. Enteric illness outbreaks reported through the national outbreak reporting system—United States, 2009–2019. *Clin. Infect. Dis.* **74**, 1906–1913 (2022).
8. Bozkurt, H., Phan-Thien, K. Y., van Ogtrop, F., Bell, T. & McConchie, R. Outbreaks, occurrence, and control of norovirus and hepatitis A virus contamination in berries: A review. *Crit. Rev. Food Sci. Nutr.* **61**, 116–138 (2021).
9. Yang, X. & Scharff, R. Foodborne illnesses from leafy greens in the united states: attribution, burden, and cost. *J. Food. Prot.* **87**, 100275 (2024).
10. Wei, J., Jin, Y., Sims, T. & Kniel, K. E. Manure- and biosolids-resident murine norovirus 1 attachment to and internalization by Romaine lettuce. *Appl. Environ. Microbiol.* **76**, 578–583 (2010).
11. Wei, J., Jin, Y., Sims, T. & Kniel, K. E. Survival of murine norovirus and hepatitis A virus in different types of manure and biosolids. *Foodborne Pathog Dis.* **7**, 901–906 (2010).
12. Alegbeleye, O. O., Singleton, I. & Sant'Ana, A. S. Sources and contamination routes of microbial pathogens to fresh produce during field cultivation: A review. *Food Microbiol.* **73**, 177–208 (2018).
13. Hirneisen, K. A. & Kniel, K. E. Norovirus surrogate survival on spinach during preharvest growth. *Phytopathology* **103**, 389–394 (2013).
14. Yeager, J. G. & O'Brien, R. T. Enterovirus inactivation in soil. *Appl. Environ. Microbiol.* **38**, 694–701 (1979).
15. Fallahi, S. & Mattison, K. Evaluation of murine norovirus persistence in environments relevant to food production and processing. *J. Food Prot.* **74**, 1847–1851 (2011).
16. DiCaprio, E., Purgianto, A. & Li, J. Effects of abiotic and biotic stresses on the internalization and dissemination of human norovirus surrogates in growing Romaine lettuce. *Appl. Environ. Microbiol.* **81**, 4791–4800 (2015).

17. Gamazo, P. et al. Modeling the transport of human rotavirus and norovirus in standardized and in natural soil matrix-water systems. *Food Environ. Virol.* **12**, 58–67 (2020).
18. Felix-Valenzuela, L., Resendiz-Sandoval, M., Burgara-Estrella, A. & Hernández, J. Mata-Haro, V. Quantitative detection of hepatitis a, rotavirus and genogroup I norovirus by RT-qPCR in fresh produce from packinghouse facilities. *J. Food Saf.* **32**, 467–473 (2012).
19. Cromeans, T. et al. Comprehensive comparison of cultivable norovirus surrogates in response to different inactivation and disinfection treatments. *Appl. Environ. Microbiol.* **80**, 5743–5751 (2014).
20. Farkas, T. et al. Genetic diversity and histo-blood group antigen interactions of rhesus enteric caliciviruses. *J. Virol.* **84**, 8617–8625 (2010).
21. Lake, A. et al. Effectiveness of Chlorine against Tulane virus, a human norovirus surrogate, and *Escherichia coli* in preharvest agricultural water. *J. Food Prot.* **88**, 100524 (2025).
22. Mirmahdi, R. S., Dicker, S. L., Yusuf, N. G. & Montazeri, N. Navigating uncertainties in RT-qPCR and plaque assay for infectivity assessment of norovirus. *Food Environ. Virol.* **17**, 22 (2025).
23. Sharma, M. et al. Survival and persistence of nonpathogenic *Escherichia coli* and attenuated *Escherichia coli* O157:H7 in soils amended with animal manure in a greenhouse environment. *J. Food Prot.* **79**, 913–922 (2016).
24. Tomás-Callejas, A. et al. Survival and distribution of *Escherichia coli* on diverse fresh-cut baby leafy greens under preharvest through postharvest conditions. *Int. J. Food Microbiol.* **151**, 216–222 (2011).
25. Baker, C. A., Lee, S., De, J., Jeong, K. C. & Schneider, K. R. Survival of *Escherichia coli* O157 in autoclaved and natural sandy soil mesocosms. *PLoS One.* **15**, e0234562 (2020).
26. Murphy, C. M. et al. Survival of twelve pathogenic and generic *Escherichia coli* strains in agricultural soils as influenced by strain, soil type, irrigation regimen, and soil amendment. *J. Food Prot.* **87**, 100343 (2024).
27. Xiong, Z. R. et al. Biological soil amendments can support survival of pathogenic and non-pathogenic *Escherichia coli* in soils and sporadic transfer to romaine lettuce. *Int. J. Food Microbiol.* **434**, 111147 (2025).
28. Abee, T., Koomen, J., Metselaar, K. I., Zwietering, M. H. & den Besten, H. M. Impact of pathogen population heterogeneity and stress-resistant variants on food safety. *Annu. Rev. Food Sci. Technol.* **7**, 439–456 (2016).
29. Gerba, C. P. & Betancourt, W. Q. Viral aggregation: impact on virus behavior in the environment. *Environ. Sci. Technol.* **51**, 7318–7325 (2017).
30. McKellar, R. C. et al. Evaluation of different approaches for modeling *Escherichia coli* O157:H7 survival on field lettuce. *Int. J. Food Microbiol.* **184**, 74–85 (2014).
31. van Boekel, M. A. J. S. On the use of the Weibull model to describe thermal inactivation of microbial vegetative cells. *Int. J. Food Microbiol.* **74**, 139–159 (2002).
32. van Boekel, M. A. J. S. To pool or not to pool: that is the question in microbial kinetics. *Int. J. Food Microbiol.* **354**, 109283 (2021).
33. Couvert, O., Gaillard, S., Savy, N., Mafart, P. & Leguérinel, I. Survival curves of heated bacterial spores: effect of environmental factors on Weibull parameters. *Int. J. Food Microbiol.* **101**, 73–81 (2005).
34. Lenth, R. Estimated Marginal Means, aka Least-Squares Means. (2024). Available at: https://CRAN.R-project.org/package=emmeans. Accessed November 22, (2024).
35. Chandler, D. & Craven, J. Relationship of soil moisture to survival of *Escherichia coli* and *Salmonella typhimurium* in soils. *Aust J. Agric. Res.* **31**, 547 (1980).
36. Ma, J., Ibekwe, M., Crowley, A., Yang, C. H. & D. E. & Persistence of *Escherichia coli* O157 and non-O157 strains in agricultural soils. *Sci. Total Environ.* **490**, 822–829 (2014).
37. Alegbeleye, O. & Sant'Ana, A. S. Survival behavior of six enterotoxigenic *Escherichia coli* strains in soil and biochar-amended soils. *Environ. Res.* **223**, 115443 (2023).
38. Park, Y., Pachepsky, Y., Shelton, D., Jeong, J. & Whelan, G. Survival of manure-borne *Escherichia coli* and fecal coliforms in soil: temperature dependence as affected by site-specific factors. *J. Environ. Qual.* **45**, 949–957 (2016).
39. Franz, E., Schijven, J., de Roda Husman, A. M. & Blaak, H. Meta-regression analysis of commensal and pathogenic *Escherichia coli* survival in soil and water. *Environ. Sci. Technol.* **48**, 6763–6771 (2014).
40. Esseili, M. A., Gao, X., Tegtmeier, S., Saif, L. J. & Wang, Q. Abiotic stress and phyllosphere bacteria influence the survival of human norovirus and its surrogates on preharvest leafy greens. *Appl. Environ. Microbiol.* **82**, 352–363 (2016).
41. Wang, G. & Doyle, M. P. Survival of enterohemorrhagic *Escherichia coli* O157:H7 in water. *J. Food Prot.* **61**, 662–667 (1998).
42. Knight, A. et al. A systematic review of human norovirus survival reveals a greater persistence of human Norovirus RT-qPCR signals compared to those of cultivable surrogate viruses. *Int. J. Food Microbiol.* **216**, 40–49 (2016).
43. Deng, W. & Gibson, K. E. Microgreen variety impacts leaf surface persistence of a human norovirus surrogate. *Food Environ. Virol.* **15**, 82–88(2023).
44. Li, D. & Uyttendaele, M. Potential of human norovirus surrogates and *Salmonella enterica* contamination of pre-harvest Basil (*Ocimum Basilicum*) via leaf surface and plant substrate. *Front. Microbiol.* **9**, 1728 (2018).
45. Wu, X., Moyne, A.-l., Ramos, T. D. M., Harris, L. J. & DiCaprio, E. Impact of irrigation water quality on human norovirus surrogate survival during leafy green production. *Front. Plant Sci.* **14**, 1128579. https://doi.org/10.3389/fpls.2023.1128579 (2023).
46. Knight, A., Li, D., Uyttendaele, M. & Jaykus, L. A. A critical review of methods for detecting human noroviruses and predicting their infectivity. *Crit. Rev. Microbiol.* **39**, 295–309 (2013).
47. Zhang, M. et al. Emerging pathogenic unit of vesicle-cloaked murine norovirus clusters is resistant to environmental stresses and UV254 disinfection. *Environ. Sci. Technol.* **55**, 6197–6205 (2021).
48. Wales, S. Q., Pandiscia, A., Kulka, M., Sanchez, G. & Randazzo, W. Challenges for estimating human norovirus infectivity by viability RT-qPCR as compared to replication in human intestinal enteroids. *Int. J. Food Microbiol.* **411**, 110507 (2024).
49. Gee, G. W. & Or, D. 2.4 Particle-Size Analysis. in *SSSA Book Series* (eds Dane, J. H. & Clarke Topp, G.) 255–293. (Soil Science Society of America, Madison, WI, USA, 2018). https://doi.org/10.2136/sssabookser5.4.c12
50. U.S. EPA & pH mlectrometric method (Method 150.1). https://www.nemi.gov/methods/method_summary/4685/ (1982).
51. U.S. EPA. Method 200.7: Determination of metals and trace elements in water and wastes by inductively coupled plasma-atomic emission spectrometry. https://www.epa.gov/esam/method-2007-determination-metals-and-trace-elements-water-and-wastes-inductively-coupled (2019).
52. U.S. EPA. EPA method 350.1: Determination of ammonia nitrogen by semi-automated colorimetry. https://www.epa.gov/esam/epa-method-3501-determination-ammonia-nitrogen-semi-automated-colorimetry (2019).
53. O'Dell, J. W. Determination of nitrate-nitrite nitrogen by automated colorimetry. in *Methods for the Determination of Metals in Environmental Samples* 464–478Elsevier, https://doi.org/10.1016/B978-0-8155-1398-8.50026-4 (1996).
54. U.S. EPA. Method 351.2, revision 2.0: determination of total Kjeldahl nitrogen by semi-automated colorimetry. https://www.epa.gov/sites/default/files/2015-08/documents/method_351-2_1993.pdf (1993).
55. U.S. EPA. Method 365.1: Determination of phosphorus by semi-automated colorimetry. https://www.epa.gov/sites/default/files/2015-08/documents/method_365-1_1993.pdf (1996).
56. FAO. Soil water content: gravimetric method. *Physical Properties*. Accessed 16 June 2025. https://www.fao.org/fileadmin/user_upload/GSP/GSDP/Field_exercises/NEW_Field_exercises/P06b-gravimetric-soil-water-EN-1-2.pdf (2016).
57. Mylavarapu, R. S. & Kennelley, E. D. Extension soil testing laboratory (ESTL) analytical procedures and training manual. *EDIS* (1969). (2002).
58. Barnes, C. et al. Application of Chitosan microparticles against human norovirus. *J. Food Prot.* **84**, 2092–2098 (2021).

59. Esseili, M. A., Wang, Q. & Saif, L. J. Binding of human GII.4 norovirus virus-like particles to carbohydrates of romaine lettuce leaf cell wall materials. *Appl. Environ. Microbiol.* **78**, 786–794 (2012).
60. U.S. FDA/U.S. EPA. Efficacy protocol for reduction of foodborne bacteria in agriculture water forpreharvest agricultural water. Protocol Review for Reg. No. 94151PA7; DP Barcode: 455973; Submission #: 1044629. (2024). https://www.fda.gov/food/food-safety-modernization-act-fsma/efficacy-protocol-reduction-foodborne-bacteria-preharvest-agricultural-water. Accessed on December 10, (2024).
61. Yusuf Garba, N. & Montazeri, N. Survival of norovirus and *Escherichia coli* in preharvest agricultural water. (International Association for Food Protection Annual Meeting, Cleveland, OH, 2025).
62. Leary, E., Young, L. J., DuClos, C. & Jordan, M. M. Identifying heat waves in Florida: considerations of missing weather data. *PLoS One*. **10**, e0143471 (2015).
63. U.S. FDA. Bacteriological Analytical Manual (BAM) Chap. 26 and Appendices: Concentration, Extraction and Detection of Enteric Viruses from Food. https://www.fda.gov/food/laboratory-methods-food/bam-chapter-26-and-appendices-concentration-extraction-and-detection-enteric-viruses-food (2022).
64. Lei, C., Yang, J., Hu, J. & Sun, X. On the calculation of $TCID_{50}$ for quantitation of virus infectivity. *Virol. Sin*. **36**, 141–144 (2021).
65. Nuanualsuwan, S. & Cliver, D. O. Pretreatment to avoid positive RT-PCR results with inactivated viruses. *J. Virol. Methods*. **104**, 217–225 (2002).
66. Sestak, K. et al. Experimental inoculation of juvenile *Rhesus macaques* with primate enteric caliciviruses. *PLoS One*. **7**, e37973 (2012).
67. Kageyama, T. et al. Broadly reactive and highly sensitive assay for Norwalk-like viruses based on real-time quantitative reverse transcription-PCR. *J. Clin. Microbiol.* **41**, 1548–1557 (2003).
68. Jothikumar, N. et al. Rapid and sensitive detection of noroviruses by using *Taq*Man-based one-step reverse transcription-PCR assays and application to naturally contaminated shellfish samples. *Appl. Environ. Microbiol.* **71**, 1870–1875 (2005).
69. Tsai, Y. L. & Olson, B. H. Rapid method for separation of bacterial DNA from humic substances in sediments for polymerase chain reaction. *Appl. Environ. Microbiol.* **58**, 2292–2295 (1992).
70. R Core Team. R: A language and environment for statistical computing. R Foundation for Statistical Computing, Vienna, Austria. https://www.R-project.org (2025).
71. Wickham, H. et al. Welcome to the tidyverse. *J. Open. Source Softw.* **4**, 1686 (2019).
72. Müller, K. here: A simpler way to find your files. R package version 1.0.1. (2024). Available at: https://CRAN.R-project.org/package=here. Accessed November 27, (2020).
73. Pinheiro, J. C. & Bates, D. M. *Mixed-Effects Models in S and S-PLUS* (Springer, 2000). https://doi.org/10.1007/b98882
74. Augustin, J. C., Carlier, V. & Rozier, J. Mathematical modelling of the heat resistance of *Listeria monocytogenes*. *J. Appl. Microbiol.* **84**, 185–191 (1998).
75. Juneja, V. K., Marks, H. M. & Mohr, T. Predictive thermal inactivation model for effects of temperature, sodium lactate, NaCl, and sodium pyrophosphate on *Salmonella* serotypes in ground beef. *Appl. Environ. Microbiol.* **69**, 5138–5156 (2003).
76. Metselaar, K. I., Besten, D., Abee, H. M. W., Moezelaar, T., Zwietering, M. H. & R. & Isolation and quantification of highly acid resistant variants of *Listeria monocytogenes*. *Int. J. Food Microbiol.* **166**, 508–514 (2013).
77. Lüdecke, D., Ben-Shachar, M., Patil, I., Waggoner, P. & Makowski, D. Performance: an R package for assessment, comparison and testing of statistical models. *JOSS* **6**, 3139 (2021).
78. Bolker, B. M. Chapter 6: likelihood and all that. In *Ecological Models and Data in R* (ed. Bolker, B. M.) 169–221 (Princeton University Press, 2008).
79. Goode, K. & Rey, K. accessed on August 29, ggResidpanel: panels and interactive versions of diagnostic plots using 'ggplot2'. R package version 0.3.0. (2024). Available at: https://cran.r-project.org/web/packages/ggResidpanel/index.html (2019).
80. Arel-Bundock, V., Greifer, N. & Heiss, A. How to interpret statistical models using marginal effects for R and python. *J. Stat. Softw.* **111**, 1–32 (2024).
81. Venables, W. N. & Ripley, B. D. *Modern Applied Statistics with S* (Springer, 2002).
82. Hothorn, T., Bretz, F. & Westfall, P. Simultaneous inference in general parametric models. *Biom J.* **50**, 346–363 (2008).
83. Graves, S., Piepho, H., Dorai-Raj, S. & multcompView Visualizations of Paired Comparisons. R package version 0.1–10. https://CRAN.R-project.org/package=multcompView (2024).
84. Schloerke, B. et al. GGally: Extension to 'ggplot2'. R package version 2.2.1. https://CRAN.R-project.org/package=GGally (2024).

Acknowledgements

We gratefully acknowledge Dr. Márcio Nunes for soil texture analysis, Mya Maybank and Ashlyn Lake for the assistance with virus recovery, Sarah Johnson for maintaining the cell lines, Anthony Crain for coordinating soil collection, and the technical insights provided by the UF/IFAS Statistical Consulting Unit.

Author contributions

Conceptualization: N.Y., K.N., S.S., M.D., K.S., N.M.; Methodology: N.Y., C.A., K.N., S.S., M.D., K.S., N.M.; Software: N.Y., N.M.; Validation: N.Y., C.A., K.N., S.S., M.D., K.S., N.M.; Formal analysis: N.Y., N.M.; Investigations: N.Y., C.A., N.M.; Resources: K.S., N.M.; Data curation: N.Y., C.A., N.M.; Writing—original draft: N.Y., C.A., N.M.; Writing - Review & Editing: N.Y., K.N., S.S., M.D., K.S., N.M.; Visualization: N.Y., N.M.; Supervision:, K.N., S.S., M.D., K.S., N.M.; Project administration: N.M.; Funding acquisition: M.D., N.M. All authors have reviewed and approved the final version of the manuscript for submission.

Funding

This study was mainly funded by the USDA National Institute of Food and Agriculture (NIFA) through the Specialty Crops Research Initiative (Award No. 2020-51181-32157). Additional funding support was provided by the Hatch Research Capacity Fund (Award No. 006540, S1077), the University of Florida startup fund, and the Archer Early Career Seed Grant. The views and interpretations presented here are those of the authors and do not necessarily represent those of the USDA.

Declarations

Competing interests

The authors declare no competing interests.

Additional information

Supplementary Information The online version contains supplementary material available at https://doi.org/10.1038/s41598-025-31728-1.

Correspondence and requests for materials should be addressed to N.M.

Reprints and permissions information is available at www.nature.com/reprints.

Publisher's note Springer Nature remains neutral with regard to jurisdictional claims in published maps and institutional affiliations.